

UAV-Based Hyperspectral Imaging of Iron(III) on Steel Infrastructure

Aaron Wickers

Chair of control engineering

HELMUT SCHMIDT UNIVERSITY/
UNIVERSITY OF THE FEDERAL ARMED FORCES

Hamburg, Germany

wickersa@hsu-hh.de

Dominik Thomas

Chair of steel structures

HELMUT SCHMIDT UNIVERSITY/
UNIVERSITY OF THE FEDERAL ARMED FORCES

Hamburg, Germany

dominik.thomas@hsu-hh.de

Dr.-Ing. Mirco Alpen

Chair of control engineering

HELMUT SCHMIDT UNIVERSITY/
UNIVERSITY OF THE FEDERAL ARMED FORCES

Hamburg, Germany

mirco.alpen@hsu-hh.de

Univ.-Prof. Dr.-Ing. Max Gündel

Chair of steel structures

HELMUT SCHMIDT UNIVERSITY/
UNIVERSITY OF THE FEDERAL ARMED FORCES

Hamburg, Germany

max.guendel@hsu-hh.de

Univ.-Prof. Dr.-Ing. Joachim Horn

Chair of control engineering

HELMUT SCHMIDT UNIVERSITY/
UNIVERSITY OF THE FEDERAL ARMED FORCES

Hamburg, Germany

joachim.horn@hsu-hh.de

Abstract— The inspection of infrastructure, such as bridges or floodgates, requires a significant human workload. The authors propose a general workflow for Unmanned Aerial System-based inspection of steel infrastructure using a hyperspectral camera to detect the spectral signature of iron(III) in rust, reducing the human workload by assigning visual inspection tasks to a UAS. A general scheme for corrosion damage derived from templates of different infrastructure operators and an algorithm for Iron(III) detection are presented. Furthermore, the paper presents an exemplary approach for UAS path planning and validates the concepts on point cloud data of the Travehafenbrücke in Hamburg, Germany.

Keywords - Inspection, UAS, Path Planning, Corrosion

I. MOTIVATION

The annual cost of corrosion is estimated to be 3 to 4% of the global gross domestic product while early and accurate corrosion detection could decrease this cost by 15 to 35% [1]. The workflow for detection can be improved by going from manual inspection labour to applying drones with automatic path planning and hyperspectral imaging, as shown in this paper. Automatic path planning takes the workload from manual flight planning from the drone operator and optimizes the inspected area per time, while the hyperspectral camera allows the detection of the specific spectral signature

of iron(III), which is a common ion occurring in atmospheric corrosion of steel.

II. INFRASTRUCTURE DIAGNOSTICS

A. German standards for corrosion and coating evaluation

As required by law, infrastructure in Germany has to be inspected completely at least every six years, including every single component as well as closed and hardly reachable areas [2].

For steel constructions the intact state of the coating protection is of special interest. Therefore, the spotted corrosion areas are documented in size and location. The evaluation of the infrastructure agencies is influenced by the standards DIN EN ISO 4628-2 bis -5. The following defects are visually inspected at a close distance of around 30 cm, according to ISO 13076 and rated into different condition classes [3]:

- Blistering according to ISO 4628-2,
- Rusting according to ISO 4628-3,
- Cracking according to ISO 4628-4,
- Delamination according to ISO 4628-5,

The aim of the MISDRO project is to automatize and objectify this currently manual task by drone inspection and image segmentation algorithms for hyperspectral images [4].

B. Defect detection from hyperspectral images

For the detection of coating defects, images are taken with a hyperspectral snapshot camera. The system is turned on and after a warm-up period of 5 minutes, a white calibration is done by flying at a height of around 1,50 cm over a Zenith Lite® Diffuse Target, 1000x1000x12 mm with an average reflectivity of 95%. Dark current calibration is done afterwards with a closed lid.

Different illumination conditions at the calibration point and inspection area lead to a different excitation spectrum, however these changes are neglected, as there are no calibration targets at the inspection side, and the illumination is expected to change the absolute values, but not the shape of the reflectance spectrum. In addition, atmospheric vapour absorption is neglected due to the close distance (< 20 m) between the image area and the sensor. The hyperspectral images are saved in a hyperspectral data cube (x, y, λ) with the spatial dimensions x, y and the corresponding wavelength λ , where one voxel contains the measured light intensity at the given spatial position and wavelength.

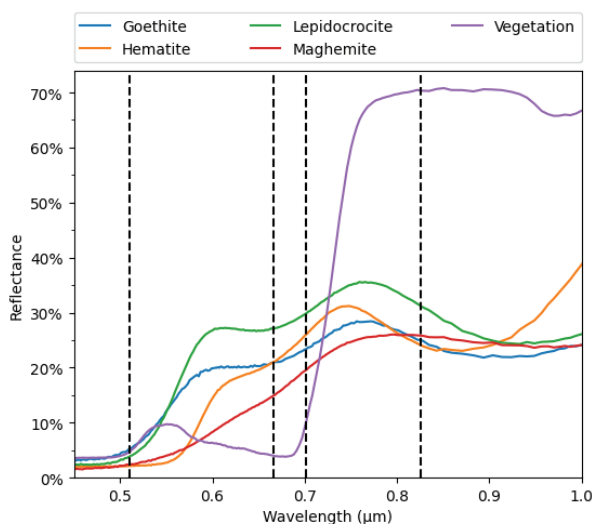


FIGURE 1. Reflectance spectra of some Iron(III)-containing minerals compared to the red edge of vegetation and selected wavelengths for hyperspectral iron(III)-detection. Values at 510, 666, 702 and 826 nm are taken for Iron(III) detection. Reflectance spectra from USGS Spectral Library 7 [5]

The atmospheric steel corrosion leads to the build-up of Iron(III)-oxides, -hydroxides and -oxide-hydroxides, where the iron(III) has specific allowed electron transitions in the optical range [6]. These electron transitions happen in the atomic shell of the iron and thus do not depend on the chemical composition and crystal structure. Exemplary spectra of iron(III) containing minerals and vegetation is shown in Figure 1. The reflectance increase in the range from 500 nm to 750 nm overlap with the reflectance increase of vegetation from 680 nm to 730 nm and has to be accounted in the analysis.

C. Spectral analysis

For the spectral analysis, several algorithms are widely applied, e.g. the Normalized Difference Vegetation Index (NDVI) or spectral angle mapper to calculate the similarity of a reflectance spectrum to spectra from a database. In this paper, we propose a simple spectral algorithm for corrosion detection in Algorithm 1.

Algorithm 1: Algorithm for iron(III) corrosion detection

input : Reflectance signal $s_\lambda = R(\lambda)$ between 0 % and 100 % of a HSI pixel at wavelength $\lambda = 510, 666, 702$ and 826 nm

output: Fe(III) index value between -1 and 1

```

1  $s_{hNDVI} = (s_{826nm} - s_{666nm}) / (s_{826nm} + s_{666nm})$ 
2 if  $s_{hNDVI} > 0.4$  then
3   | return -1 /* vegetation */
4  $s_{hNDFe3I} = (s_{702nm} - s_{510nm}) / (s_{702nm} + s_{510nm})$ 
5 return  $s_{hNDFe3I}$ 

```

The algorithms gives each spatial pixel a value between -1 and 1, with higher values indicating higher possible iron(III) content. Vegetation is filtered out by using a hyperspectral NDVI. In this case, spatial pixels with NDVI values greater 0.4 indicate a healthy vegetation and are therefore ignored [7]. The used wavelengths can also be found in Figure 1.

Spatial pixels given higher Iron(III) indicating values than 0.4 are taken as corrosion. An example image is given in Figure 2. The image shows two disadvantages of the simple algorithm: First, the top left corner contains highlighted spatial pixels, with a wrong calibration, because the white reference target did not cover the whole image during calibration. Second, the upper half of the image detected some spatial pixels of the sky as possible corrosion areas, due to a backlight increase, leading to wrong reflectance values above 100%. Both issues can be addressed by filtering out spatial pixels above this threshold.

By using the field of view of the camera and distance to the area of interest, the physical size of the corroded area can be determined and used for evaluation according to the rust grade in ISO 4628-3.

III. UAS & SENSORS

The following section presents the sensor and UAS setup deployed, enabling a fast and inexpensive inspection of the structure without the need for long closure intervals with regard to the specific inspection requirements.

A. Hyperspectral camera

The MISDRO project employs a Cubert Ultris X20 Plus as a hyperspectral snapshot camera with a weight of 630 g, dimensions of 86x121x105 mm, 640x640 spatial pixels, 164 spectral bands from 350 to 1000 nm with 4 nm spectral sampling and a FWHM of 10 nm each. Each pixel has a dynamic range of 12 bit.

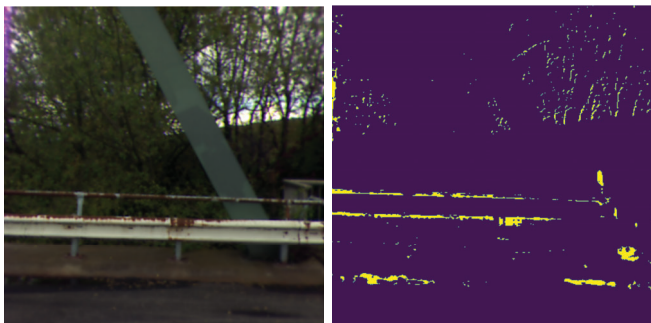


FIGURE 2. RGB-representation of an hyperspectral image of corroded areas on a bridge (left) and potential iron(III)-containing pixels marked by algorithm 1 (right)

The spatial resolution is increased via pansharpening, by using a 1886x1886 pixel greyscale sensor from a second camera mounted on top of the first.

The camera employs light field technology resulting in a minimum distance of 6 m to the AOI for matching pixel signals. The minimum distance can be adjusted by recalibration with a specific calibration target. The field of view is 35°. Data readout is done by global shutter with a maximum frame rate of 4 Hz and allowed integration times between 0.1 and 1000 ms. The maximum power consumption is 8 Watt.

B. UAS

For an inspection mission with the hyperspectral camera introduced in chapter III-A a sufficient UAS has to be developed. Therefore, the requirements and the solution are addressed in the following section. Different aspects have to be considered for the concept of a UAS. Favourably, the UAS for an inspection mission should be as compact as possible to reduce the dimensions and therefore create a better accessibility regarding the infrastructure. Further, a long flight time is beneficial to reduce maintenance time and a stable, yet agile flight behaviour is necessary to ensure the reliable recording of hyperspectral images. However, the UAS has to be able to lift the inspection sensor with the associated gimbal and has to hold other sensors for navigation purposes as well. Finally, the UAS should be capable to record images at any angle such that the UAS can access a desired inspection point from above or below. Balancing this variety of different interests, we developed a UAS with the dimensions of 860x860x700 mm. The UAS is capable to lift 3 kg additional payload corresponding to the approximated 1.5 kg for an inspection sensor mounted on a gimbal and another 1.5 kg for a LIDAR, which is used for navigation purposes. The total weight adds up to about 12.5 kg, including a battery pack of 10 Ah ensuring a total flight time of at least 15 min. The UAS is designed with four arms and eight coaxial rotors in X-configuration as depicted in Figure 3. Also, the c-shaped construction around the centre of the UAS is shown, which holds the LIDAR and the camera gimbal on opposite sides. This unique part solves the mentioned issue of ensuring images to be taken from above and below. During an exchange

of the battery pack the construction can be rotated by 180° for taking images in the other direction. This construction ensures an overall compact design granting the benefits of the stable flight behaviour of a well-known multicopter. Further to mention, the UAS is equipped with a *Pixhawk 6X FCU*, a *Gigabyte BRIX* onboard pc and common telemetry- and GPS-modules. The onboard pc is used for sensor fusion and the control of the hyperspectral camera. The communication is based on ethernet and ROS2. The UAS's dimensions are used to create a collision model, which also takes the different mounting options into account. Therefore, the models' height differs with ± 30 cm. The models will be considered for path planning and collision avoidance purposes.



FIGURE 3. Rendering of the developed UAS with the C-shaped sensor-mounting

IV. PATH PLANNING

The proposed UAS design has major influence on the mission planning that will be briefly discussed in the following. For more information about the used algorithms, the reader is encouraged to follow the upcoming publications of the authors. Note that the rotation of the c-shaped construction has to be considered during the process. The mission planning therefore creates two separate missions for points approached from above and below the UAS. Only one of them will be visualized in the results.

The general concept of the path planning is depicted in fig. 4. Starting from a point cloud recorded at the infrastructure or a BIM model, an algorithm performs an extraction of the most significant surfaces of the model. The precision can be customized and is also depending on the point cloud density or the overall quality of the underlying data. Considering the derived sensor model of the hyperspectral camera relevant inspection points are placed among the extracted surfaces with respect to a certain overlap between the individual images. With the help of the collision model of the UAS and the infrastructure model waypoints in the \mathbb{R}^3 are created. An optimization algorithm takes into account hard constraints such as an unblocked line of sight and a collision-free spacing towards the structure but also factors like the viewing angle, the distance to the desired inspection point and lighting conditions. After the best fitting waypoints have been evaluated, they are sorted for separate missions depending on the mounting of

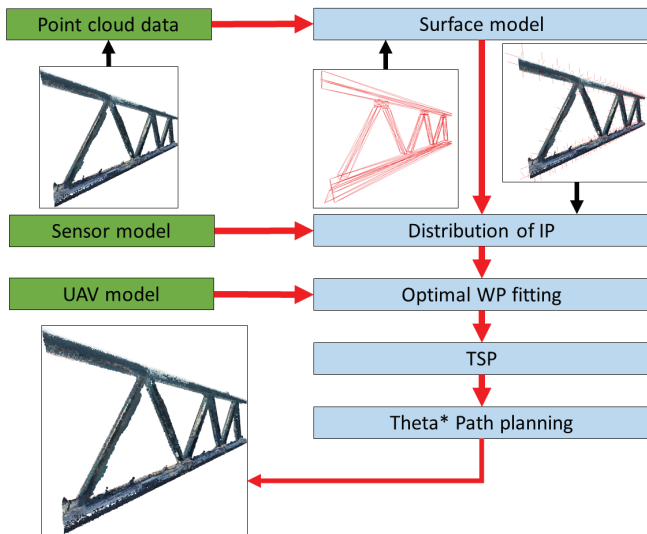


FIGURE 4. Visualization of the general workflow of the mission planning

the camera. The missions further are processed by a Travelling Salesman Problem (TSP) with an approximated Euclidean distance to optimize for path length and therefore required inspection time. Finally, a *Theta** algorithm calculates an exact path for the sorted mission, which then is handed to the UAS. An exemplary 3D visualization of an inspection of three bridge elements extracted from the Travehafenbrücke located at the port of Hamburg, Germany, is shown in Figure 6. A 2D representation with respect to the $x-y$ - and the $x-z$ -plane is depicted in Figure 5. The mission is calculated for the introduced UAS with the hyperspectral camera mounted on the bottom. The red lines indicate the path and the dashed black lines roughly show the outlines of the bridge. The graph shows a meandering path in the $x-y$ -plane to inspect the upper side of the bridge. Further, with respect to a certain safety distance, waypoints along the sides of the bridge are taken into account. The groups of points in the middle of the left tile are placed in the small areas inside the triangular structures, that allow the UAS to maintain the required safety distance. Those points can also be recognized in the $x-z$ -plane depicted in the right tile of the figure. This tile however mainly shows the full vertical coverage of the bridge. Since the algorithm presented is restricted to movements along a grid, small adjustments of the path are necessary to move between the navigation grid and the exact waypoints for the inspection. Our current work focuses on improvements for a smoother path by implementing a cluster algorithm, that combines nearby waypoints into a single waypoint. Also, the current direction of movement will be taken into account to eliminate unnecessary changes of the paths' direction. However, the result shows an appropriate path for a UAS with respect to a predefined safety distance derived from the UAS model. The presented work can easily be adapted to other sensors such as RGB- or thermal cameras and other UAS configurations or collision models.

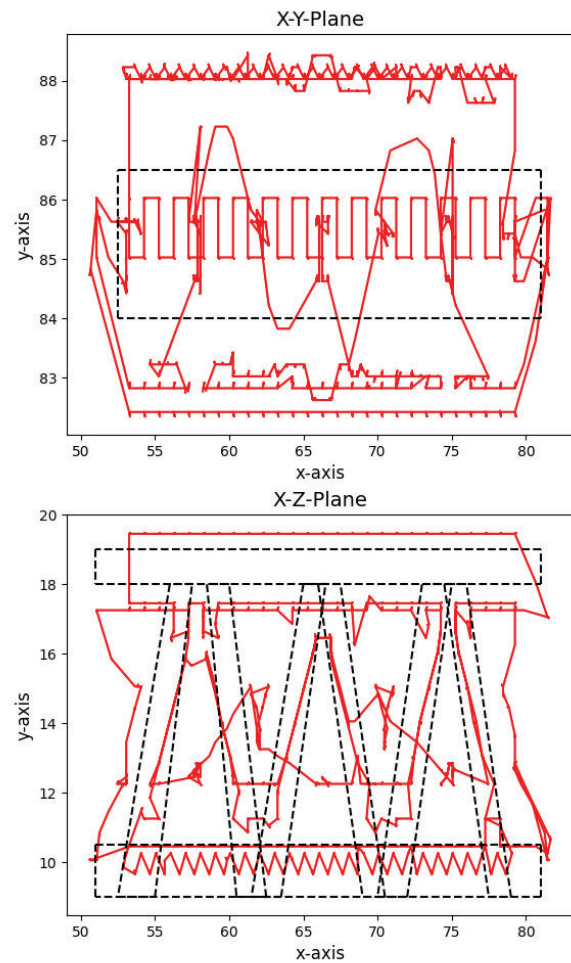


FIGURE 5. 2D Visualization of an inspection mission with the HSI camera mounted below in the X-Y-Plane (top) and X-Z-Plane (bottom)

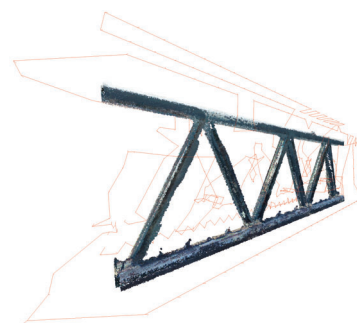


FIGURE 6. 3D Visualization of the inspection mission from fig. 5

V. CONCLUSION

In this paper the authors present algorithms and the rudimentary concept of a UAS, that are capable to detect surfaces on a building and inspect those automatically with a mounted hyperspectral camera. Also an algorithm for the evaluation of the gathered data is presented, such that the detection of iron(III) from atmospheric steel corrosion according to ISO 4628-3 is possible. The proposed algorithm takes the increase of iron(III) and vegetation between 650 nm and 850 nm into consideration, while different illumination conditions between the calibration target and inspection area are neglected.

The current path planning is not optimized yet and will be improved in the future. Cluster algorithms and other optimizations will therefore be taken into account to achieve a much smoother and thus more reasonable path. However, the deployed system is already capable of reducing the closure times for inspection missions and reduce the costs and the effort of the necessary maintenance procedures. The authors work will focus on improvements and evaluation for the given algorithms. Test scenarios on real infrastructures with the presented system are planned for the near future.

ACKNOWLEDGMENT

This research paper and the project MISDRO are funded by dtec.bw – Digitalization and Technology Research Centre of the Bundeswehr which we gratefully acknowledge. dtec.bw is funded by the European Union – NextGenerationEU.

REFERENCES

- [1] NACE IMPACT. “International Measures of Prevention, Application, and Economics of Corrosion Technology Study”. In: *NACE Int* (2016).
- [2] Iris Hindersmann and Stefan Staub. “Herausforderungen für ein Lebenszyklusmanagement für Bauwerke der Verkehrsinfrastruktur – Ergebnisse von leitfadengeführten Experteninterviews”. In: *Bautechnik* 99.11 (2022), pp. 817–824.
- [3] *Beschichtungsstoffe – Beleuchtung und Durchführung für visuelle Abmusterungen von Beschichtungen*. Norm. Feb. 2020.
- [4] Dominik Thomas et al. “Drohngestützte, multivariate Inspektionssysteme zur Zustandserfassung von Stahlbrücken und Stahlwasserbauten”. In: (2022).
- [5] RF Kokaly et al. “Usgs spectral library version 7 data: Us geological survey data release”. In: *United States Geological Survey (USGS): Reston, VA, USA* 61 (2017).
- [6] Dominik Thomas and Max Gündel. “Hyperspectral imaging systems for corrosion detection from remotely operated vehicles”. In: *ce/papers* 6.5 (2023), pp. 934–938.
- [7] Andrés Viña, Geoffrey M. Henebry, and Anatoly A. Gitelson. “Satellite monitoring of vegetation dynamics: Sensitivity enhancement by the wide dynamic range vegetation index”. In: *Geophysical Research Letters* 31.4 (2004).